
Micro-Macro Transition and Simpler Contact Models for Wet Granular Materials

Sudeshna Roy · Abhinendra Singh · Stefan Luding · Thomas Weinhart

Received: date / Accepted: date

Abstract Wet granular materials in steady-state in a quasi-static shear flow have been studied with discrete particle simulations. Macroscopic fields, consistent with the conservation laws of continuum theory, are obtained by time averaging and spatial coarse-graining. Initial studies involve understanding the effect of liquid content and liquid properties like the surface tension on the macroscopic fields. Two parameters of the liquid bridge contact model have been studied as the constitutive parameters that define the structure of this model (i) the rupture distance of the liquid bridge model, which is defined by the liquid content, and (ii) the maximum adhesive force which is controlled by the surface tension of the liquid. Subsequently a correlation is devel-

oped between these micro parameters and the macroscopic cohesive strength in the limit of zero pressure. The macroscopic cohesive strength of the non-linear liquid bridge contact model scales well with the cohesive strength for a simple linear irreversible contact model with the same constitutive micro parameters at equal energy dissipated per contact. Finally, the macroscopic torque measured at the walls, which is an experimentally accessible parameter, is calculated from our simulation results.

1 Introduction

Granular media are collections of microscopic grains having athermal interactions through dissipative, frictional or cohesive contact forces. External force leads to granular flow under the condition of applied shear stress exceeding the yield shear stress. After a finite shear strain, at constant rate, a steady state establishes with a typically lower shear stress, depending on both strain rate and pressure [1]. Most studies in granular physics focus on dry granular materials and their flow rheology. However, wet granular materials are ubiquitous in geology and many real world applications where interstitial liquid is present between the grains. We study the local rheology of weakly wetted granular materials in the quasistatic regime using the Discrete Element Method (DEM) in a shear cell set-up, where the relative motion is confined to particles in a narrow region away from the walls, called shear band [2, ?]. The pendular regime exists in partially saturated granular system with a very low level of water content, where the formation of liquid bridges between the particles leads to development of microscopic tensile forces. This tensile forces generated at particle level results in cohesion

S. Roy
Multi Scale Mechanics (MSM), Engineering Technology (CTW) and MESA+, University of Twente
P.O.Box 217, 7500 AE Enschede, The Netherlands
Tel.: +31-(0)53 489-3301
E-mail: s.roy@utwente.nl

A. Singh
Multi Scale Mechanics (MSM), Engineering Technology (CTW) and MESA+, University of Twente
P.O.Box 217, 7500 AE Enschede, The Netherlands
Tel.: +31-(0)53 489-2694
E-mail: a.singh@utwente.nl

S. Luding
Multi Scale Mechanics (MSM), Engineering Technology (CTW) and MESA+, University of Twente
P.O.Box 217, 7500 AE Enschede, The Netherlands
Tel.: +31-(0)53 489-4212
E-mail: s.luding@utwente.nl

T. Weinhart
Multi Scale Mechanics (MSM), Engineering Technology (CTW) and MESA+, University of Twente
P.O.Box 217, 7500 AE Enschede, The Netherlands
Tel.: +31-(0)53 489-3301
E-mail: t.weinhart@utwente.nl

at macroscopic scale. Earlier studies have been done for the pendular regime of liquid bridge to understand the effect of liquid bridge volume and contact angle on different macroscopic fields like cohesive strength, torque and shear band properties [3, 4, 5, 6, 7]. Other studies for unsaturated granular media says about fluid depletion in shear bands [8, 9]. However, there is no theoretical framework or concrete model available yet that defines the exact correlation between the micro parameters like the liquid bridge volume and the surface tension of the liquid with the macroscopic cohesive strength.

In order to develop a micro-macro correlation for the liquid bridge contact model, we initially study the structure of the micro contact model. How is the structure of the liquid bridge contact model affected by the microscopic parameters? How does this influence the macroscopic cohesive strength? We do a details study on the effect of these parameters on the macro results to know this. For example, the effect of maximum interaction distance or the distance at which the liquid bridge between two interacting particles ruptures is studied by varying the liquid content. On the other hand other parameters like surface tension of the liquid and contact angle affects the magnitude of force acting between the particles when in contact [16, 5]. Various surface tension of liquids give a large scale variation of the capillary force and this gives us the motivation to study the effect of surface tension on the macro properties.

The liquid bridge interaction between the particles are defined by the free-surface equilibrium shapes and stability of the bridge configuration between them [10]. Phenomenologically even the simplified models of liquid bridges are quite complex in nature. In order to improve the computational efficiency for wet granular materials, we replace the non-linear interactions of liquid bridges with a simpler linear one. But in what way can a non-linear model like the liquid bridge contact model be replaced by a linear model? When can we say that the two different contact models are analogous? Therefore, we compare the realistic liquid bridge model with an equivalent simple linear irreversible contact model [11] that would give the same macroscopic effect.

The results in this paper are organized in three main parts. In Sec. 3.1 of this paper we study the effect of varying liquid bridge volume and surface tension of the liquid on the macroscopic properties, the focus being to find a micro-macro correlation from this study. Most strikingly, we see a well defined relationship between these micro parameters and the macro properties like the steady state cohesive strength of the bulk material and macro-torque required under shear, neglecting the effect of fluid depletion in shear bands [8, 9] in quasistatic flow. In Sec. 3.2 of this paper we show the

derivation of macro torque from the boundary shear stress. In this section we also compare this torque with the torque calculated from forces due to contacts on the wall particles. In Sec. 4 of this paper, we discuss about the analogy of two different contact models, with a goal to understand which parameters at microscopic scale would give the same macroscopic behavior of the system.

2 Model System

2.1 Geometry

Split- Bottom Ring Shear Cell: The set-up used for simulations consists of a shear cell with annular geometry and a split in the bottom plate, as shown in figure 1. The geometry of the system consists of an outer cylinder (radius $R_o = 110$ mm) rotating around a fixed inner cylinder (radius $R_i = 14.7$ mm) with a rotation frequency of $f_{rot} = 0.01$ s⁻¹. The granular material is confined by gravity between the two concentric cylinders, the bottom plate, and a free top surface. The bottom plate is split at radius $R_s = 85$ mm into a moving outer part and a static inner part. Due to the split at the bottom, a shear band is formed at the bottom, it moves inwards and widens as it goes up, due to the geometry. This set-up thus features a wide shear band away from the wall, free from boundary effects, since an intermediate filling height ($H = 40$ mm) is chosen, so that the shear band does not reach the inner wall at the free surface.

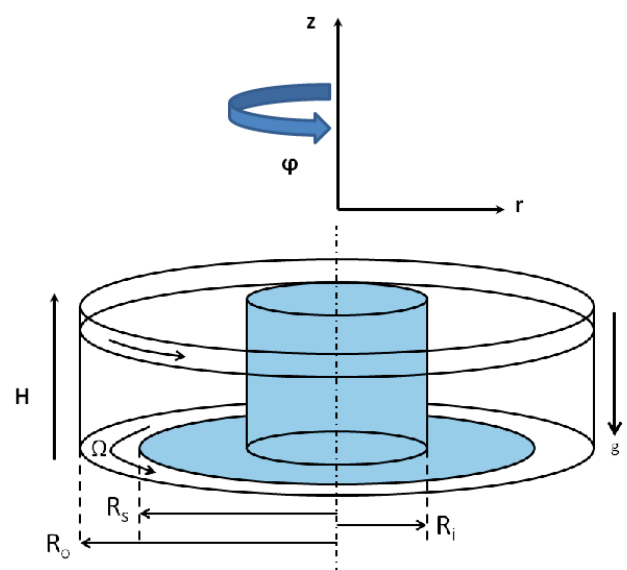


Fig. 1 Shear cell set-up

In our previous work [12], the simulations were done using a quarter of the system ($0^\circ \leq \phi \leq 90^\circ$) using periodic boundary conditions. In order to save computation time, here we simulate only a section of the system ($0^\circ \leq \phi \leq 30^\circ$) with the same periodic boundary conditions in the angular coordinate, unless specified otherwise. We have observed no noticeable effect on the macroscopic behavior in comparisons between simulations done with the smaller (30°) and the larger (90°) opening angle.

2.2 Microscopic model parameters

Cohesion is a phenomenon of inter-molecular forces that hold the particles of a substance together. In liquid medium, cohesion is caused by the unbalanced inward pull on the molecules of the liquid at the surface which is a result of the surface tension of the liquid. On the other hand the cohesion between grains with liquid is assumed to originate from the liquid bonds which depend on the total liquid volume. Therefore, we choose to vary these characteristic elements of a liquid bridge model to understand the behavior of macroscopic cohesion. All the fixed interaction parameters for the contact models [1, 12] are given in appendix A. All the variable interaction parameters like the liquid bridge volume V_b and the surface tension of liquid γ are discussed in this section.

2.2.1 Bulk saturation and liquid bridge volume

The bulk material can be divided into different states such as the dry bulk, adsorption layers, pendular state, funicular state, capillary state or suspension depending on the level of saturation [13, 14]. In this paper we intend to study the phenomenology of liquid bridge between particles in the pendular state, where the well separated liquid bridges exist individually without geometrical overlap. In this section, we discuss about the critical bulk saturation of granular materials and the corresponding liquid bridge volumes in the pendular state.

The bulk saturation S^* is defined as the ratio of liquid volume to void volume of the bulk [15]. The demarcation between the pendular state and the more saturated funicular state is given by the saturation $S^* \approx 0.3$ [15]. For each particle pair with a liquid bridge, a dimensionless volume φ^* can be defined as the ratio of the volume of the liquid bridge at the contact, V_b to the volume of the two contacting particles, $2V_p$:

$$\varphi^* = \frac{V_b}{2V_p} = \frac{V_b}{2 \cdot \frac{\pi}{6} d_p^3} \quad (1)$$

Assuming the liquid is homogeneously distributed throughout the material, the bulk saturation S^* is obtained from the dimensionless volume φ^* and the bulk porosity ϵ from the following equation:

$$S^* = \pi \frac{1 - \epsilon}{\epsilon^2} \varphi^* \quad (2)$$

With a bulk porosity of the material $\epsilon = 0.4$ and an average particle diameter d_p of 2.2 mm, the transition volume of liquid bridge is approximately found to be 284 nl. In order to study the influence of liquid content on the macroscopic properties, we analyzed the system for the following set of liquid bridge volumes V_b :

$$V_b \in [0, 1, 2, 4.2, 8, 14, 20, 75, 140, 200] \text{ nl} \quad (3)$$

which are seen to be well within the pendular regime. In order to investigate the functional form of cohesive strength beyond this state, a few more simulations for higher V_b are done:

$$V_b \in [500, 1000, 5000, 10000] \text{ nl} \quad (4)$$

2.2.2 Surface tension of liquid

Surface tension results from the greater attraction of liquid molecules towards each other than towards air. It is the elastic tendency of liquids which makes it acquire the least possible surface area with higher inter liquid-molecules attraction. As a result, cohesive properties of liquids is reflected in surface tension which makes it an interesting parameter to study. The details of its effect on microscopic capillary force will be discussed in details in Sec. 2.3.1. The effect of surface tension on the macroscopic properties is studied for the following range of surface tension values:

$$\gamma \in [0, 0.020, 0.040, 0.060] \text{ Nm}^{-1} \quad (5)$$

Surface tension of most of the liquid-air interface at 20°C are in this range. To investigate the functional behavior of cohesive strength beyond this state, a few more simulations for higher γ are done:

$$\gamma \in [0.10, 0.50, 1.00, 5.00] \text{ Nm}^{-1} \quad (6)$$

2.3 Contact models

2.3.1 Liquid bridge capillary force model

The capillary pressure difference sustained across the liquid-air interface due to surface tension can be described by the non-linear Laplace-Young equation [10]. The capillary force in a pendular bridge originate from the axial component of this force. Another component

that contributes to the capillary force is the from the hydrostatic pressure. Many previous studies have reported calculation of capillary forces based on numerical solution of the Laplace-Young equation and also by experimental results [10,16]. The magnitude of liquid bridge capillary force depends on the volume of the liquid bridge between the particles, the contact angle θ , surface tension γ , the effective radius of the particles r_{eff} and the inter-particle distance S equal to $-\delta$, the overlap between the particles. With these parameters we approximate the inter-particle force f_c of the capillary bridge according to the proposal of [16]. The experimental results are fitted by a polynomial to obtain the capillary forces as a function of the scaled separation distance. During approach of the particles, the normal contact force for this model is given by:

$$f = \begin{cases} 0 & \text{if } S < 0; \\ -f_c^{max} + f_n & \text{if } S \geq 0; \end{cases} \quad (7)$$

During separation of the particles, the normal contact force for this model is given by:

$$f = \begin{cases} 0 & \text{if } S > S_c; \\ f_c & \text{if } S < 0; \\ -f_c^{max} + f_n & \text{if } S \geq 0. \end{cases} \quad (8)$$

where

$$f_c = \frac{2\pi\gamma r \cos \theta}{1 + 1.05\bar{S} + 2.5\bar{S}^2} \quad (9)$$

$$\bar{S} = S \sqrt{\frac{r}{V_b}} \quad (10)$$

$$f_c^{max} = 2\pi\gamma r \cos \theta \quad (11)$$

The effective radius of two spherical particles of different size can be estimated as the harmonic mean of the two particle radii according to the Derjaguin approximation [17], yielding the effective radius:

$$r = \frac{2r_i r_j}{r_i + r_j} \quad (12)$$

The normal contact repulsive force is given by:

$$f_n = k\delta \quad (13)$$

The contact and non-contact forces for interacting particles can be described by a combination of an elastic contact model for the normal repulsive force and a non-linear irreversible adhesive model for the adhesive force. Figure 4 represents a sketch of the combined liquid bridge contact model. The liquid bridge adhesive

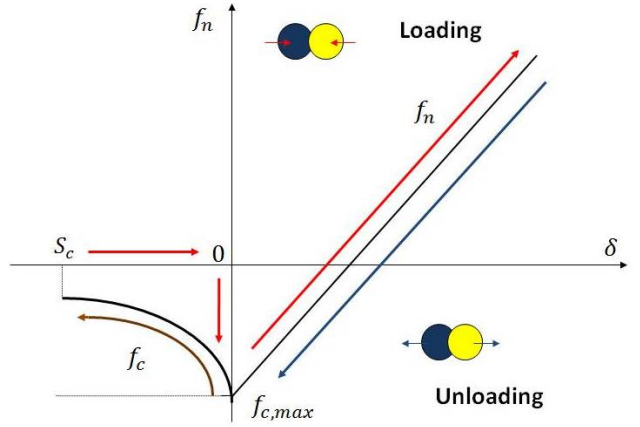


Fig. 2 Liquid capillary bridge model. The red lines represent the loading direction, the blue line represents the unloading direction when the particles are in contact and the brown line represents the unloading for the non-contact particles with short-range interaction force.

force acts between the particles once the contact is established between the particles. This model equation is applicable for mono-disperse particles [3,16] which has been actually extended to poly-disperse system of particles in Ref. [5]. When the particles are in contact with overlap, the attractive force is given by Eq. 11. This is independent of the liquid bridge volume and depends on the surface tension of the liquid, radius of particles and contact angle. There is no cohesive force between the particles during approach. As the liquid bridge only forms once the particles come in contact with each other, the cohesive force starts acting and remains constant during overlap between particles $\delta > 0$. The liquid bridge capillary force decreases in magnitude with increase in separation distance between the particles as given by Eq. 9. As proposed by [18], the critical separation distance S_c between the particles before the bridge ruptures is given by:

$$S_c = \left(1 + \frac{\theta}{2}\right) V_b^{1/3} \quad (14)$$

The liquid bridge capillary force as a function of separation distance is shown in figure 3 for different volume of liquid bridges. The rupture distance is a function of $V_b^{1/3}$ as stated in Eq. 14.

2.3.2 Linear irreversible contact model

In Sec. 4 we introduce a simple linear irreversible contact model as proposed by [11] which can be compared with the non-linear liquid bridge interaction model. During approach of the particles, the normal contact force

Table 1 Non-dimensionalization of parameters

Parameter	Symbol	Scaling term
Capillary force	f_c	f_g
Shear stress	τ	f_g/d_p^2
Pressure	P	f_g/d_p^2
Macroscopic cohesive strength	c	f_g/d_p^2
Liquid bridge volume	$V_b^{1/3}$	d_p
Surface tension	γ	f_g/d_p
Scaled cohesive strength	c/γ^α	$f_g^{(1-\alpha)}/d_p^{(2-\alpha)}$
Rupture distance	S_c	d_p
Torque	T^z	$f_g R_o$
Angular rotation	θ_{rot}	$2\pi\omega t_{max}$
Scaled torque	T'	$f_g^{(1-\alpha)}/d_p^{(2-\alpha)}$
Adhesive Energy	E	$f_g d_p$
Scaled cohesive strength	c/γ^β	$f_g^{(1-\beta)}/d_p^{(2-\beta)}$

of interstitial liquid between the particles in the pendular regime, cohesive force acts between the particles which increases with increase in volume of liquid bridge. This results in the macroscopic cohesive strength c as given by Eq. 17.

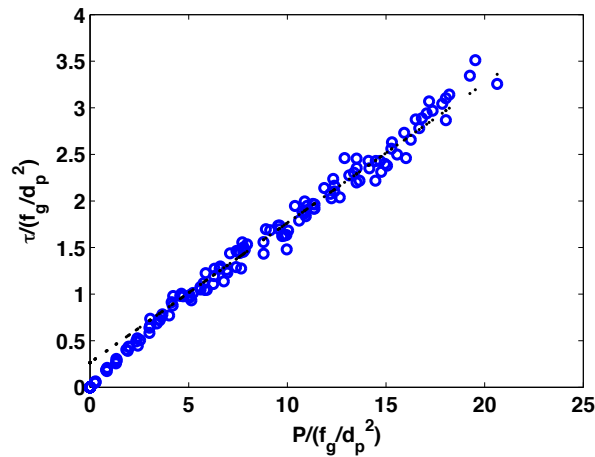


Fig. 5 Shear stress τ scaled in terms of f_g/d_p^2 plotted against pressure P scaled in terms of f_g/d_p^2 . The dotted line represents the fitting function as given by Eq. 17 for $P > 100$ Pa where, $\mu = 0.15$ is the macroscopic friction coefficient, $c = 5.973$ for $V_b = 75$ nl and $\gamma = 0.020$ Nm^{-1} .

Earlier studies on wet granular materials have shown that the presence of liquid bridges between the particles result in an increase in macroscopic cohesive strength of the materials [3, 4, 12, 6]. The question arises regarding how the variation of liquid bridge volume and the properties of the materials like e.g. surface tension affect the macroscopic cohesive strength. Our earlier studies show the macroscopic cohesive strength c as a function of liquid bridge volume. It was found to increase non-linearly with increase in volume of liquid bridge. Here, the co-

hesive strength is studied in detail, including very small volumes of liquid bridge, including the (practically impossible) limit of 0 nl liquid bridge volume as given in Eq. 3. Theoretically there is a finite cohesive strength for 0 nl liquid bridge volume. This is due to the microscopic capillary bridge force that acts between particles even at 0 nl liquid bridge volume as given by Eq. 11. This is called the critical cohesive strength c^* for a given surface tension of liquid. This is a function of the maximum force acting between two particles when they are in contact as given by Eq. 11 and is constant for any volume of liquid bridge. The additional cohesive strength for higher volume of liquid bridge is due to the non-contact capillary forces between the particles that are active between the particles till the liquid bridge ruptures. This is a function on the surface tension of the liquid and the volume of the liquid bridge. Thus, the cohesive strength of granular materials for a given liquid bridge volume can be written as:

$$c = c^* + c' \quad (18)$$

where c^* is the critical cohesive strength corresponding to 0 nl liquid bridge volume and is a function of the surface tension of the liquid. c' is the additional cohesive strength for liquid bridge volume $V_b > 0$ and is a function of the liquid bridge volume and surface tension. Figure 6a) shows c' as a linear function of $V_b^{1/3}$. Eq. 14 shows rupture distance S_c as a linear function of $V_b^{1/3}$. Therefore, substituting c' as a linear function of S_c , Eq. 18 is written as:

$$\frac{c}{f_g/d_p^2} = \frac{c^*}{f_g/d_p^2} + a(S_c/d_p) + b \quad (19)$$

where a and b depends on the surface tension of the liquid.

Figure 6b) shows the macroscopic cohesive strength is plotted as a function of surface tension for a volume of

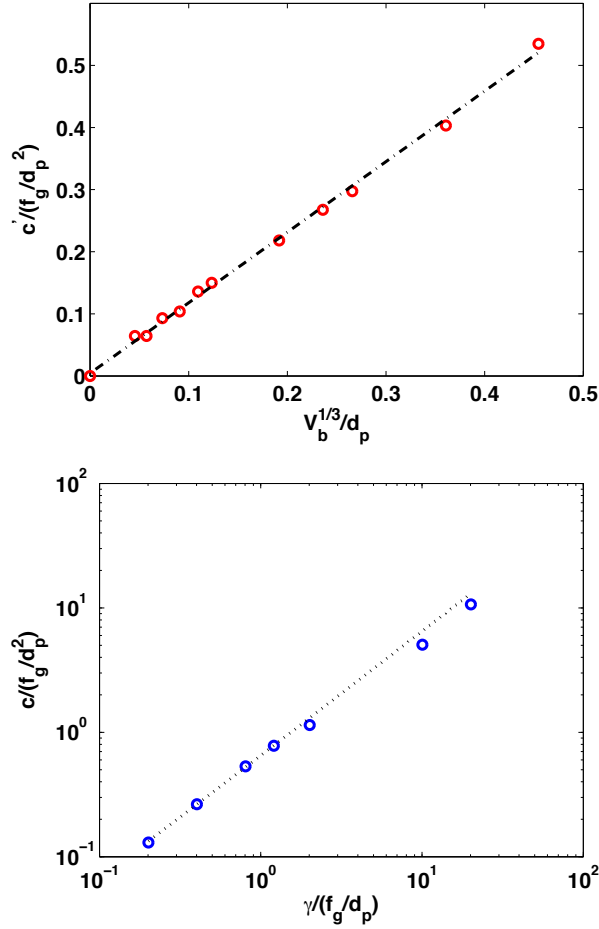


Fig. 6 a) c' scaled in terms of f_g/d_p^2 as a function of $V_b^{1/3}$ scaled in terms of mean particle diameter d_p for $\gamma = 0.020 \text{ Nm}^{-1}$. The dotted line represents the fitting function $\frac{c'}{f_g/d_p^2} = 1.1361(V_b^{1/3}/d_p) + 0.0042$. b) Macroscopic cohesive strength c scaled in terms of f_g/d_p^2 as a function of surface tension γ scaled in terms of f_g/d_p for $V_b = 75 \text{ nl}$, γ is scaled in terms of f_g/d_p where f_g is the gravitational force and d_p is the mean particle diameter. The dotted line represents the fitting function given by Eq. 20.

75 nl liquid bridge. As shown in figure 6b), the cohesive strength is linearly proportional to the liquid surface tension, and can be described from the fitting line of figure 6b) by:

$$\log\left(\frac{c}{f_g/d_p^2}\right) = \alpha \log\left(\frac{\gamma}{f_g/d_p}\right) + k \quad (20)$$

where $\alpha \approx 1.0031$, $k = -0.1841$ Eq. 20 may be alternatively written as:

$$\frac{c}{f_g/d_p^2} = b'' \left(\frac{\gamma}{f_g/d_p}\right)^\alpha \quad (21)$$

where b'' is obtained from the fitting constant k in Eq. 20. For higher surface tension of liquid, the results deviate from the fitted function of linear dependence as seen

from the figure. On the other hand, the macroscopic friction coefficient increases ($\mu > 0.15$) with increase in surface tension of liquid. As given by Eq. 19 and 20, the macroscopic cohesive strength is a function of liquid bridge volume expressed in terms of maximum interaction distance S_c between the particles and the maximum adhesive force expressed in terms of surface tension of the liquid γ . So in the later sections of this paper we express macroscopic parameters as a function of the micro parameters S_c representing interaction distance and γ representing maximum force for all contact models.

The macroscopic cohesive strength scaled by surface tension is plotted as function of the rupture distance for different surface tension as shown in figure 7. The scaled cohesive strength is a linear function of the rupture distance as shown in the figure. This can be fitted in a straight line equation given by:

$$\frac{c/\gamma^\alpha}{f_g^{(1-\alpha)}/d_p^{(2-\alpha)}} = p(S_c/d_p) + q \quad (22)$$

where $p = 2.1977$ and $q = 0.1646$ are obtained from the fitting function in figure 7. The coefficients are obtained from the fitting function in figure 7. The characteris-

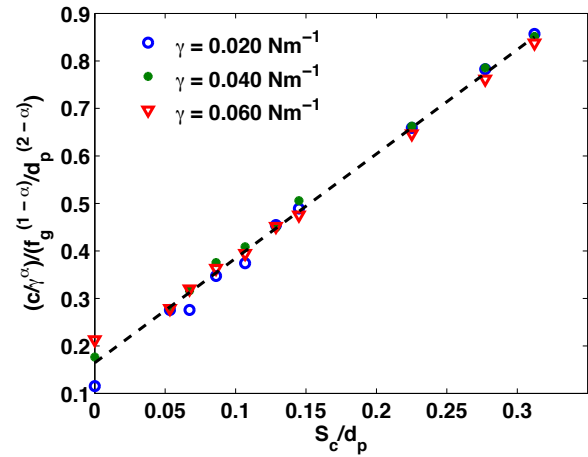


Fig. 7 c/γ^α scaled in terms of $f_g^{(1-\alpha)}/d_p^{(2-\alpha)}$ as a function of the rupture distance S_c scaled in terms of particle diameter d_p . The dotted line represents the fitting function given by Eq. 22.

tics of the liquid bridge model that varies with surface tension of the liquid is the maximum interacting force between the particles. Similarly, we see a variation in interacting distance between the particles with change in liquid bridge volume or rupture distance. So these are the parameters of the liquid bridge capillary force model that affects the macroscopic cohesive strength.

3.2 Macroscopic torque analysis from the microscopic parameters

The torque applied on the shear cell wall to rotate it with a constant angular velocity depends on the yield shear stress on the boundary walls. Loosely speaking, torque is a measure of the shear stress or force acting on the particles at the wall and thus can be used to find an estimate of shear stress at the outer wall. Certainly, torque should have a strong connection with the cohesion in the system. To study solely the effect of capillary cohesion on the torque, the other parameters like the microscopic friction is kept very small in our simulations with $\mu_{micro} = 0.01$. Earlier studies of [4] shows that the average torque acting on the rotating part of the shear cell increases with increase in liquid bride volume. In this section we do a details analysis of the macroscopic torque as a function of the micro parameters in order to understand its connection with the cohesive strength of the material.

In order to show the evolution of torque as a function of the rotational angle θ , we compare our results with the experimental results as given by [23]. Figure 8 shows the numerically calculated torque as a function of angular rotation θ . This is in agreement with the angular rotation required for steady state torque evolution as given in [23], considering the difference in magnitude of torque due to different rotation rate and due to different friction in the system.

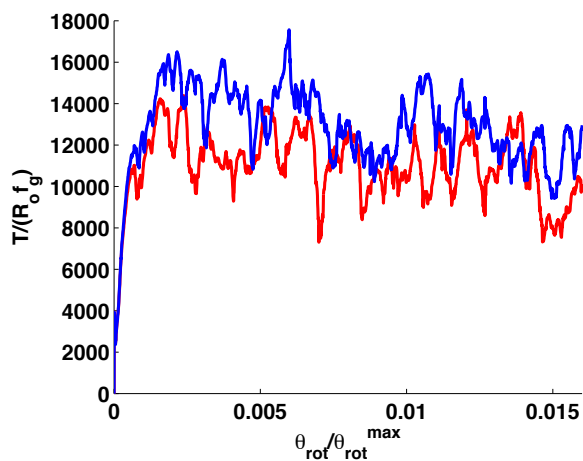


Fig. 8 Torque scaled in terms of $f_g R_o$ as a function of angular rotation θ_{rot} scaled in terms of $\theta_{rot}^{max} = 2\pi\omega t_{max}$, where $\omega = 0.01 \text{ s}^{-1}$, $t_{max} = 200 \text{ s}$, for surface tension of liquid $\gamma = 0.020 \text{ Nm}^{-1}$ for $V_b = 4 \text{ nl}$ (red) and $V_b = 200 \text{ nl}$ (blue).

The torque is calculated based on the contact forces on the fixed particles on the moving part (outer) and

stationary part (inner) of the shear cell. Thus the net torque inner and outer torque are calculated by summing up the torque for all the contact forces of the outer wall and inner wall particles respectively, with respect to the axis of rotation of the shear cell. The net torque is obtained from the difference between the outer wall torque and the inner wall torque. We multiply the total torque by a factor of $\frac{2\pi}{\pi/6}$ in order to get the torque for the whole system from the obtained torque of our simulations in 30° section. Thus the torque is given by:

$$\hat{T} = \left(\sum_{i=1}^N \sum_{j \in R} c_{i,j} \times \hat{f}_{i,j} \right)_{outer} - \left(\sum_{i=1}^N \sum_{j \in R} c_{i,j} \times \hat{f}_{i,j} \right)_{inner} \times \frac{2\pi}{\pi/6} \quad (23)$$

where N represents the number of particles, R is the set of all particles forming the outer wall and base plate of the shear cell, \hat{c}_{ij} is the position of the contact point and \hat{f}_{ij} is the interacting force. Since we do simulation on a 30° section of the shear cell, we multiply the torque with a factor of 12 in Eq. 23 to calculate the torque for the whole system. Only the z-component of the resultant torque are analyzed and is denoted as T^z , as we want to study the torque required to shear the materials in φ direction. Figure 9 shows T^z as a function of the surface tension of liquid as given by figure . We observe that the resultant torque increases linearly with increase in surface tension of the liquid.

The scaled equation of torque are written as:

$$\frac{T'}{f_g^{(1-\alpha)}/d_p^{(2-\alpha)}} = e(S_c/d_p) + f \quad (24)$$

$$T' = \left(\frac{T^z}{t/(\mu P_{avg})} - \mu P_{avg} \right) / \gamma^\alpha \quad (25)$$

where $e = 2.0864$ and $f = 0.1937$, t is the fitting parameter obtained from figure 9 and P_{avg} is the average pressure equal to 260 Pa based on shear cell height of about 17 times the particle diameter.

Our results show that the coefficients given by Eq. 19 for macroscopic cohesive strength and that given by Eq 24 for macroscopic torque are quite the same. This shows that the two macroscopic parameters shares an inter-relation between them.

4 An analogous linear irreversible contact model for cohesive particles

In this section we discuss about finding the key microscopic parameters for a linear irreversible contact model

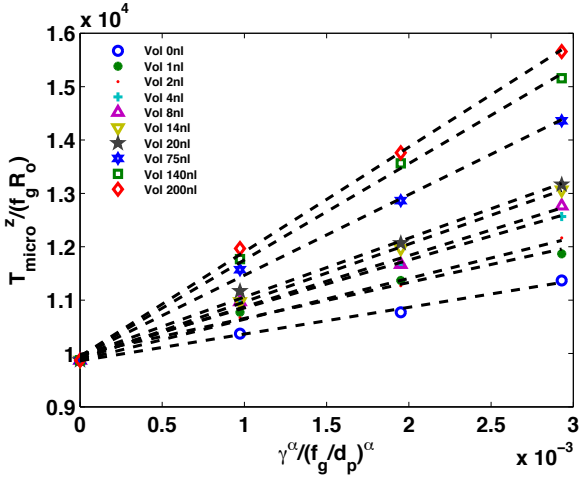


Fig. 9 Torque T^z scaled in terms of $f_g R_o$ as a function of surface tension of liquid γ^α scaled in terms of $(f_g/d_p)^\alpha$ where f_g is the gravitational force, R_o is the outer radius of the shear cell and d_p is the mean particle diameter. The dotted lines represent the fitting functions for different volumes of liquid bridge given by equation $\mathbf{T}^z/(f_g R_o) = l \frac{\gamma^\alpha}{(f_g/d_p)^\alpha} + t$ where $t = 9.9279 \times 10^3$ and l increases with increase in volume of the liquid.

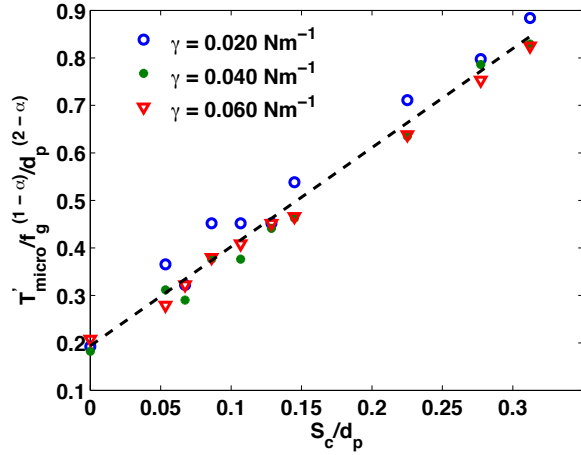


Fig. 10 T' scaled in terms of $f_g^{(1-\alpha)}/d_p^{(2-\alpha)}$ as a function of rupture distance S_c scaled in terms of particle diameter d_p for different surface tension of liquid where T' is given by Eq. 25. The dotted line represents the fitting function as given by Eq. 24.

[11] that is macroscopically analogous to liquid bridge contact model. An explanation of the linear irreversible contact model used for this comparison is explained in [11]. Unlike the liquid bridge contact model, the force for the linear irreversible contact model is simple and independent of polydispersity in the system. Figure 11 shows the force-overlap distribution for the two contact models showing the loading and unloading directions of forces which are irreversible.

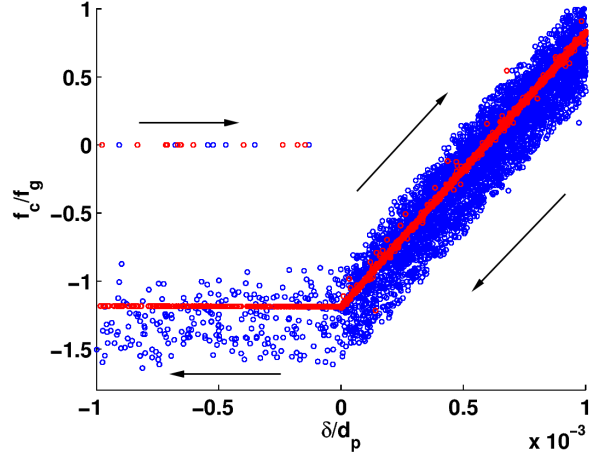


Fig. 11 Force-overlap diagram for the linear-irreversible contact model (red) as compared with the liquid bridge model (blue). The arrow shows the loading and the unloading directions for all forces.

As discussed in section 3.1, the macroscopic cohesive strength for the liquid bridge model are defined by the rupture distance of the liquid bridge which is dependent on the liquid bridge volume and the magnitude of maximum interaction force which is governed by the surface tension of the liquid. Assuming that the non-linear liquid bridge capillary force can be replaced by a simple irreversible linear adhesive force between the particles with the same macro characteristics with an equivalent microscopic characteristics, we compare the cohesive strength of the two models as explained in Sec. 4.1.

4.1 An approach towards equal maximum force and equal interaction distance

The key parameters that define the cohesive force of a linear irreversible contact model are the maximum adhesive force and the adhesive stiffness. Several simulations have been run for the linear irreversible contact model in the same numerical set-up with the same maximum adhesive force as the liquid bridge model and adhesive stiffness that would result in the same interaction range for different volumes of liquid bridge for different surface tension of liquid. The adhesive stiffness that are equivalent to the liquid bridge volumes as given by Eq. 3 for different surface tension as given by Eq. 5. For surface tension of liquid 0.020 Nm^{-1} the adhesive stiffness for different volumes of liquid are:

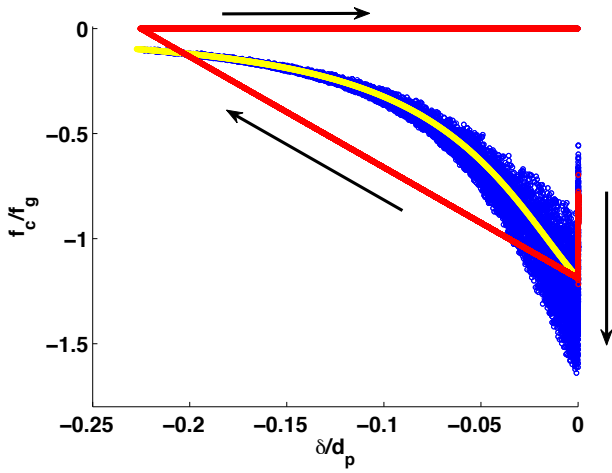


Fig. 12 Adhesive force f_c scaled in terms of gravitational force f_g as a function of overlap δ scaled in terms of mean particle diameter d_p linear irreversible contact model (red) as compared with the liquid bridge model (blue) for equal maximum force and equal interaction distance. The yellow line represents the liquid bridge contact model for mean particle diameter d_p . The arrow shows the loading and the unloading directions for the short-range forces.

$$k_{adh} \in [1.11, 0.88, 0.69, 0.56, 0.46, 0.41, 0.26, 0.21, 0.19] Nm^{-1} \quad (26)$$

The results of macroscopic cohesive strength c as scaled by surface tension of liquid γ for the liquid bridge model (blue) and linear irreversible model with equal maximum force and equal interaction distance are shown in figure 14. The results are not really analogous as seen from the figure as the intercepts for the fitting lines of the two models are different. However, the fitting lines for the two different contact models are parallel. The fitting parameters for the liquid bridge contact model shown in the figure is given by:

$$\frac{c/\gamma^\alpha}{f_g^{(1-\alpha)}/d_p^{(2-\alpha)}} = g(S_c/d_p) + h \quad (27)$$

$g = 2.1716$ and $h = 0.1370$ for liquid bridge contact model, $g = 2.0984$ and $h = 0.3407$ for linear irreversible contact for surface tension $\gamma = 0.020 Nm^{-1}$. The fitting coefficients are obtained from the dotted and solid lines respectively in figure 14.

So for a given volume of liquid bridge and a given surface tension of liquid, the linear irreversible contact model with the same maximum force and same interaction distance has a higher cohesive strength.

4.2 An approach towards equal maximum force and equal adhesive energy

Efforts are made to find an analogous linear irreversible contact model for a given liquid bridge contact model by equalizing the maximum force and interaction distance for the models as discussed in section 4.1. However, the cohesive strength for the two models depend differently on the interaction distance for a given maximum force. Now, approaches are made to quantify the equivalent intensity of cohesion for the two contact models with an equal maximum adhesive force and equal adhesive energy E . The adhesive energy for a given contact model is obtained by the total area under the force-overlap distribution in figure 13. A linear analogous for the liquid bridge contact model is obtained with the equal maximum force with surface tension $0.020 Nm^{-1}$ and the adhesive stiffness adjusted to have the equal adhesive energy as given by:

$$k_{adh} \in [\infty, 2.95, 2.11, 1.49, 1.10, 0.84, 0.74, 0.39, 0.29, 0.25] Nm^{-1} \quad (28)$$

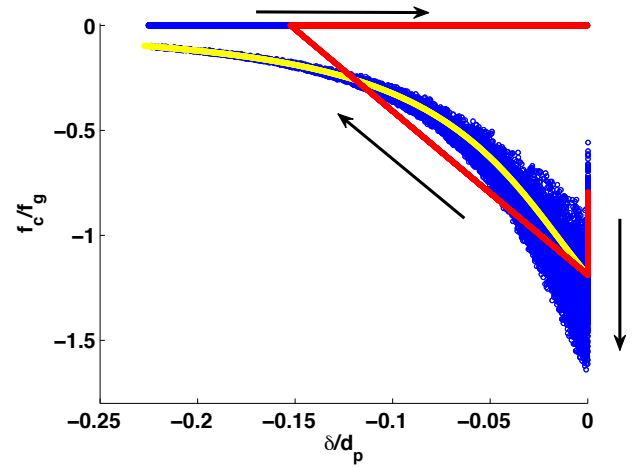


Fig. 13 Adhesive force f_c scaled in terms of gravitational force f_g as a function of overlap δ scaled in terms of mean particle diameter d_p for linear irreversible contact model (red) as compared with the liquid bridge model (blue) for equal maximum force and equal adhesive energy. The yellow line represents the liquid bridge contact model for mean particle diameter d_p . The arrow shows the loading and the unloading directions for the short-range forces.

The force-overlap for contacts with $\delta < 0$ for the two comparable contact models with equal adhesive energy are shown in figure 13. Figure 14 shows c/γ^α as a function of rupture distance S_c for the liquid bridge model (blue) of surface tension $\gamma = 0.020 Nm^{-1}$ compared

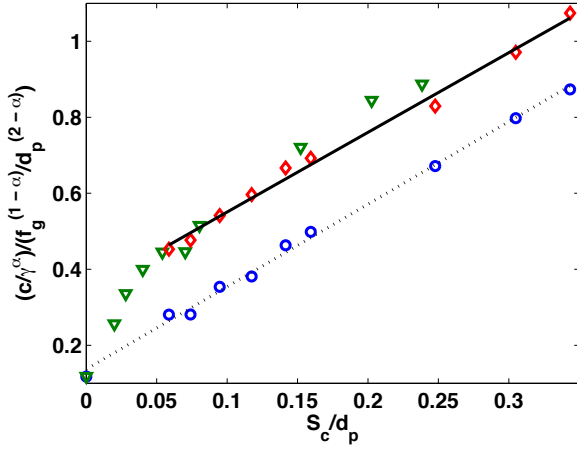


Fig. 14 c/γ^α scaled in terms of $f_g^{(1-\alpha)}/d_p^{(2-\alpha)}$ as a function of the rupture distance S_c scaled in terms of mean particle diameter d_p for the liquid bridge model (blue) and the linear irreversible model with equal interaction distance (red) and equal adhesive energy (green) for $\gamma = 0.020 \text{ Nm}^{-1}$. The dotted and the solid lines represent the fitting function given by Eq. 27.

with the two cases of linear irreversible contact model with equal interaction distance (red) and equal energy (green). The linear irreversible model with equal energy as the liquid bridge model has a lower interaction distance. So the functional behavior of cohesive strength for the linear irreversible contact model for small interaction range can be understood from this. As observed from figure 14, this is a non-linear function of the interaction distance S_c at low interaction distance and becomes linear for higher range.

Figure 15 shows the cohesive strength as a function of total adhesive energy for the liquid bridge model (blue) of surface tension $\gamma = 0.020 \text{ Nm}^{-1}$ compared with the two cases of linear irreversible contact model with equal interaction distance (red) and equal energy (green). As seen from the figure, for a given maximum force which is determined by the surface tension of the liquid, the macroscopic cohesive strength c is equal for the the liquid bridge model and the linear irreversible model with equal energy. The cohesive strength for the linear irreversible model with equal interaction distance is higher as it has higher adhesive energy than the liquid bridge model. However, all the data for the three cases as explained above collapse and functionally they behave the same.

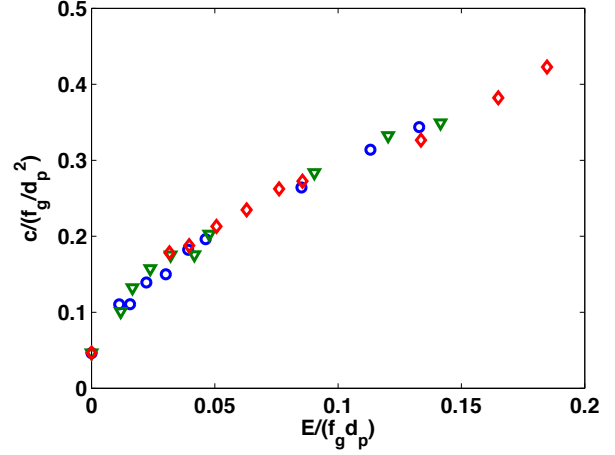


Fig. 15 c scaled in terms of f_g/d_p^2 as a function of adhesive energy E scaled in terms of $f_g d_p$ for the liquid bridge model (blue) and the linear irreversible model with equal interaction distance (red) and equal adhesive energy (green) for $\gamma = 0.020 \text{ Nm}^{-1}$.

4.3 An approach towards different maximum force for the two contact models

In the earlier sections, results show that for a given maximum force and it is observed that the cohesive strength for the two contact models functionally behave the same under various conditions. To study the functional order for the two models under different maximum force conditions, we study the macroscopic behavior of the linear model for different surface tension. Simulations equivalent to surface tension 0.040 Nm^{-1} and 0.060 Nm^{-1} are run with an equivalent adhesive stiffness 2 times and 3 times of that given by Eq. 26 keeping the interaction distance same. Figure 16 shows a comparison of the force-overlap for the two contact models for surface tension of liquid 0.020 Nm^{-1} and 0.040 Nm^{-1} .

Figure 17a) shows a plot of macroscopic cohesive strength as a function of total adhesive energy dissipated by the particles per contact for different surface tension for the liquid bridge model and linear model. For the same energy dissipated per contact, a higher surface tension of liquid results into a higher macroscopic cohesion. From figure 17b), for a given surface tension of liquid γ , the macroscopic cohesive strength is given by:

$$\frac{c/\gamma^\beta}{f_g^{(1-\beta)}/d_p^{(2-\beta)}} = u(E/f_g d_p)^2 + v(E/f_g d_p) + w \quad (29)$$

where E is the adhesive energy dissipated per contact for the corresponding contact model, and $\beta \approx 0.33$, u

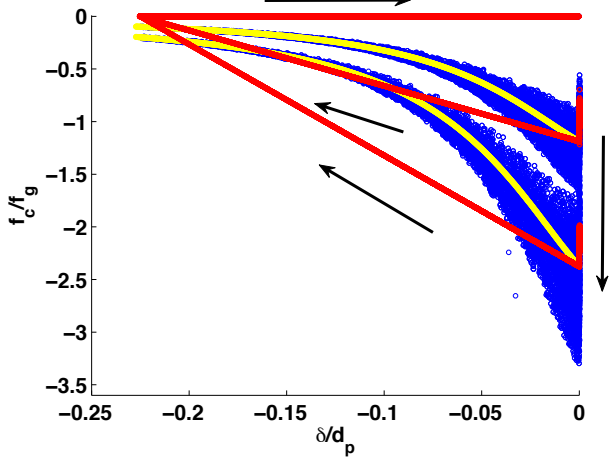


Fig. 16 Adhesive force f_c scaled in terms of gravitational force f_g as a function of overlap δ scaled in terms of mean particle diameter d_p for linear irreversible contact model (red) as compared with the liquid bridge model (blue) for different maximum force and equal interaction distance. The yellow lines represent the liquid bridge contact model for mean particle diameter d_p . The arrow shows the loading and the unloading directions for the short-range forces.

$= -1.8802$, $v = 2.6447$ and $w = 0.1614$ as obtained from the fitting function in figure 17.

5 Conclusion

We obtained a fitting correlation to obtain the macroscopic cohesive strength for the liquid bridge model for given microscopic parameters. The parameters that define the structure of the liquid bridge contact model are the volume of the liquid bridge, surface tension of liquid and the contact angle. A detailed study on the effect of liquid bridge volume and surface tension of liquid is done in this paper. Both these microscopic parameters control the cohesion in wet granular materials in different ways. We found that the macro cohesive strength of the system is linearly dependent on the maximum force e.g. the surface tension is one of the parameters that controls the maximum force of liquid bridge. On the other hand we found that the macro cohesive strength is also linearly dependent on the maximum interacting distance between the particles which depends on the volume of the liquid bridge. From these results we have obtained a good micro-macro correlation for the liquid bridge model.

We have analyzed the effect of cohesion on the torque required to rotate the system at a given rotation rate which is another macroscopic property of the system. It is observed that the torque and the macro cohesive strength of the system are well related and show similar

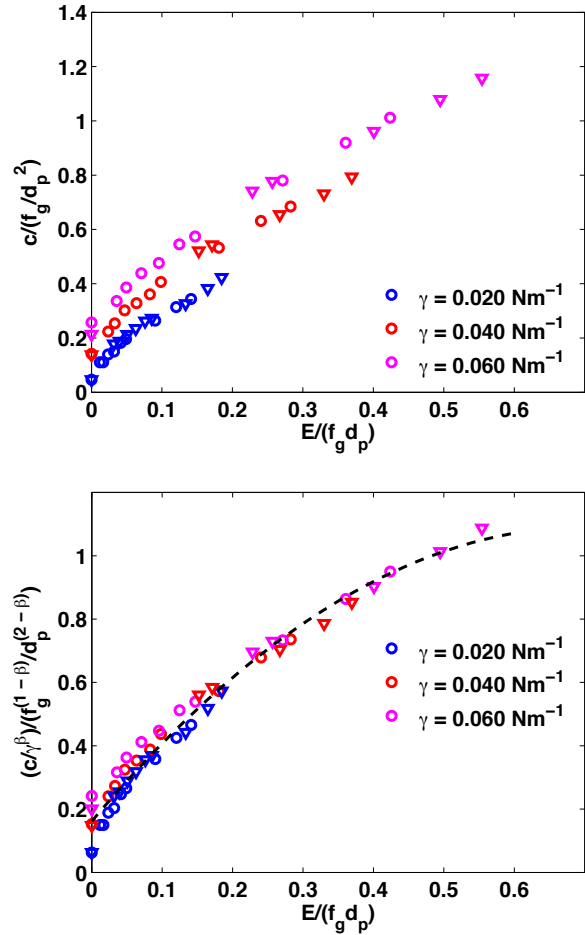


Fig. 17 a) c scaled in terms of f_g/d_p^2 as a function of adhesive energy E scaled in terms of $f_g d_p$ for different surface tension of liquid. b) Macroscopic cohesive strength c/γ^β scaled in terms of $f_g^{(1-\beta)}/d_p^{(2-\beta)}$ as a function of adhesive energy E scaled in terms of $f_g d_p$ for different surface tension of liquid as compared with the linear irreversible model. The dotted line represents the fitting function is given by the Eq. (29). Different symbols denote \circ liquid bridge model and ∇ linear irreversible model.

linear dependence (slope and offset) on the microscopic parameters.

An analogy is established between the liquid bridge model and a simple linear irreversible contact model. These two models have different micro-macro correlations. However, we found that the macroscopic cohesive strength for the two models are same if the maximum force and the total adhesive energy for the two models are the same, irrespective of the nature of attractive force acting between the particles. In this way we can always replace non-linear liquid bridge force for the system and obtain the macroscopic properties from an analogous linear adhesive model that takes less computational time. Results for different magnitude of maximum force of the two models show that they behave

functionally different for different magnitude of maximum force. The two types of contact models with equal energy and different magnitude of maximum force have different macroscopic cohesive strength. So equal adhesive energy dissipated per contact is not the sole microscopic condition for the two contact models to be analogous. However, overall a correlation is obtained between the cohesive strength and the microscopic parameters like the maximum force and the total adhesive energy dissipated per contact. This correlation is shown to hold good for any irreversible adhesive contact model.

In this paper our results are focused on the micro-macro correlations and comparing different contact models. However, it would be interesting to study the forces and their distribution for wet cohesive system. Our future study will be focused on understanding the microscopic origin of the force network and statistics of the inter-particle forces inside a shear band.

A Appendix

Key contact model parameters

Sliding friction coefficient μ 0.01

Elastic stiffness k 120 Nm⁻¹

Viscous dissipation coefficient η 0.001

Angular frequency ω 0.01 s⁻¹

Acknowledgements We thank Prof. R. Schwarze and A. Gladkyy for useful discussions. Financial support through the "Hydrodynamic theory of wet particle systems: Modeling, simulation and validation based on microscopic and macroscopic description" project of STW is acknowledged.

References

1. A. Singh, V. Magnanimo, K. Saitoh, S. Luding, Physical Review E **90**(2), 022202 (2014)
2. P. Schall, M. van Hecke, Ann. Rev. Fluid Mech. **42** (2010)
3. R. Schwarze, A. Gladkyy, F. Uhlig, S. Luding, Granular matter **15**(4), 455 (2013)
4. A. Gladkyy, R. Schwarze, Granular Matter **16**(6), 911 (2014)
5. S. Herminghaus*, Advances in Physics **54**(3), 221 (2005)
6. V. Richefeu, M.S. El Youssoufi, F. Radjai, in *Theoretical and Numerical Unsaturated Soil Mechanics* (Springer, 2007), pp. 83–91
7. P. Darabi, T. Li, K. Pougatch, M. Salcudean, D. Grecov, Chemical Engineering Science **65**(15), 4472 (2010)
8. R. Mani, D. Kadau, D. Or, H.J. Herrmann, Physical review letters **109**(24), 248001 (2012)
9. R. Mani, D. Kadau, H.J. Herrmann, Granular Matter **15**(4), 447 (2013)
10. F. Soulie, F. Cherblanc, M.S. El Youssoufi, C. Saix, International journal for numerical and analytical methods in geomechanics **30**(3), 213 (2006)
11. A. Singh, V. Magnanimo, S. Luding, Powder Technol (2013)
12. S. Roy, S. Luding, T. Weinhart, Procedia Engineering (2015)
13. N. Mitarai, F. Nori, Advances in Physics **55**(1-2), 1 (2006)
14. A. Denoth, Journal of Glaciology **28**(99), 357 (1982)
15. T. Weigert, S. Ripperger, Particle & Particle Systems Characterization **16**(5), 238 (1999)
16. C.D. Willett, M.J. Adams, S.A. Johnson, J.P. Seville, Langmuir **16**(24), 9396 (2000)
17. B. Deryaguin. Untersuchungen über die reibung und adhäsion, iv, theorie des anhaftens kleiner teilchen (1934)
18. G. Lian, C. Thornton, M.J. Adams, Journal of colloid and interface science **161**(1), 138 (1993)
19. S. Luding, Particulate Science and Technology **26**(1), 33 (2007)
20. S. Luding, Particuology **6**(6), 501 (2008)
21. S. Luding, Computer Physics Communications **147**(1), 134 (2002)
22. A. Singh, V. Magnanimo, K. Saitoh, S. Luding, arXiv preprint arXiv:1412.0874 (2014)
23. G.H. Wortel, J.A. Dijksman, M. van Hecke, Physical Review E **89**(1), 012202 (2014)